Digital Transportation and Safety

ARTICLE

Open Access

https://doi.org/10.48130/dts-0026-0009

Digital Transportation and Safety **2026**, 5(2): 111–122

Cooperative control method for freeway ramp merging in mixed traffic environments

Tao Wang[1], Huichuan Deng[1], Wu Ning[2], Yanming Fang[3], Jianghua Li[4] and Yuan Luo[4*]

[1] *School of Architecture and Transportation Engineering, Guilin University of Electronic Technology, Guilin, Guangxi 541004, China*
[2] *Guangxi Beibu Gulf International Port Group Co., Ltd, Nanning, Guangxi 530201, China*
[3] *Beijing Wanji Technology Co., Ltd, Beijing 100193, China*
[4] *Guangxi Computing Center Co., Ltd, Nanning, Guangxi 530022, China*
* Correspondence: luoyuan_pro@foxmail.com (Luo Y)

Abstract

Highway on-ramp merging in mixed traffic environments, where connected and automated vehicles (CAVs) coexist with human-driven vehicles (HDVs), remains challenging due to the stochastic and non-cooperative behaviors of HDVs. This paper proposes a hierarchical optimization framework for cooperative on-ramp merging, in which the problem is formulated as a two-layer structure. The decision-making layer optimizes cooperative merging strategies, while the optimal control layer generates vehicle trajectories. To enable decision search and trajectory computation in the proposed model, a Monte Carlo Tree Search-based Hamiltonian algorithm (MCTS-H) is designed. SUMO-based simulation experiments are conducted to validate the proposed framework and algorithm under varying traffic demands and CAV penetration rates, with evaluation from the perspectives of traffic efficiency and traffic flow stability. In terms of traffic efficiency, MCTS-H consistently outperforms the no-control and proportional-integral-derivative (PID) baselines. Under high congestion with 60% CAV penetration, it reduces average vehicle delay by 68.92% and 24.67%, respectively. From the perspective of traffic flow stability, spatiotemporal trajectory analysis further confirms that MCTS-H eliminates extreme acceleration events induced by HDV maneuvers, thereby achieving a more stable traffic flow. These results demonstrate that the proposed method is effective in addressing the cooperative on-ramp merging problem.

Keywords: Ramp merging control, Mixed traffic environments, Monte Carlo Tree Search, Optimal control, Connected and automated vehicles

Citation: Wang T, Deng H, Ning W, Fang Y, Li J, et al. 2026. Cooperative control method for freeway ramp merging in mixed traffic environments. *Digital Transportation and Safety* 5(2): 111–122 https://doi.org/10.48130/dts-0026-0009

Introduction

Highway ramp merging areas are critical bottlenecks in freeway systems, where vehicle interactions often lead to congestion and safety risks[1]. Early studies mainly focused on macroscopic control strategies, such as ramp metering and variable speed limits[2], which improve efficiency but are inherently limited by the lack of fine-grained perception and vehicle-level coordination. With the development of vehicle-to-everything communication technologies, connected and automated vehicles (CAVs) offer a promising solution for mitigating merging congestion. However, the stochastic and non-cooperative behaviors of human-driven vehicles (HDVs) pose significant challenges to ramp merging in mixed traffic environments. Consequently, developing effective ramp merging strategies has become a key research topic.

Current research on ramp merging control has predominantly focused on pure CAV environments, with studies demonstrating its superiority over traditional macroscopic methods[3]. These approaches are broadly categorized into rule-based and optimization-based methods. Rule-based methods focus on priority assignments to coordinate vehicle interactions. For instance, Chen et al.[4] and Ding et al.[5] focused on improving computational efficiency, while Hou et al.[6], Peng et al.[7], and Li et al.[8] validated and extended the feasibility of such methods in complex. Optimization-based methods typically formulate merging as an optimal control problem. Rios-Torres et al.[9] developed a model with acceleration as the objective function, aiming to improve efficiency in the control zone. Hu & Sun[10] formulated a joint optimization problem to manage the vehicle lane-changing and trajectories. Building upon existing optimization models, Zhou et al.[11,12] introduced receding horizon to resolve the merging problem. Meanwhile, Zhao et al.[13] shifted their focus toward dampening traffic oscillations. While these strategies are highly effective at enhancing traffic efficiency in pure CAV environments, their performance degrades in mixed traffic environments.

To address the limitations of pure CAV environments, cooperative merging control in a mixed traffic environment has emerged as a key technical pathway. This approach typically treats HDV behaviors as optimization constraints to generate trajectories for creating and utilizing safe merging gaps. Representative works include: Chen et al.[14], who formulated the problem as a mixed-integer nonlinear programming model to co-optimize discrete sequences and continuous trajectories, though the NP-hard complexity hinders real-time application. Ntousakis et al.[15] formulated the merging scenario as a finite-horizon optimal control problem, solving it via a model predictive control approach; however, its assumption of a pure CAV environment limits direct use in a mixed traffic environment. Xue et al.[16] used a grey prediction model to forecast vehicle state and available gap on the mainline, but the system is confined to choosing pre-existing gaps without active coordination. Similarly, Yang et al.[17] proposed a safety-oriented method with a bi-level gap selection function, yet it relies on passive cooperation from mainline CAVs and overlooks trade-offs among comfort and fuel economy. Lastly, Cheng et al.[18] combined Monte Carlo Tree Search (MCTS) with optimal control for global optimization in a mixed traffic environment. Nevertheless, their work lacks an analysis of the collaborative modes and mechanisms between CAVs and HDVs.

Existing research on on-ramp merging control in mixed traffic environments has two critical limitations. First, the available gap is typically limited to existing safe spaces on the mainline, without actively coordinating mainline vehicles to create better merging opportunities[19]. Secondly, while most methods treat enhancing traffic efficiency as their single objective, they overlook the crucial aspect of traffic flow stability.

To address the above-mentioned problem, this study proposes a hierarchical cooperative merging framework, solved by a designed Monte Carlo Tree Search-Hamiltonian (MCTS-H) algorithm. This approach is designed to determine the optimal available gap and cooperative maneuvers for merging vehicles, ultimately aiming to enhance traffic efficiency and ensure traffic flow stability.

In summary, the main contributions of this paper are listed below:

(1) Propose a hierarchical cooperative merging framework in mixed traffic environments that actively creates merging gaps by decoupling discrete decisions from continuous control.

(2) Develop the MCTS-H algorithm, which makes decisions via a kinematically enhanced MCTS and generates trajectories using a Hamiltonian-based analytical trajectory solver, thereby ensuring decision feasibility and trajectory smoothness.

(3) The proposed hierarchical cooperative merging framework and MCTS-H algorithm are validated through comprehensive case studies, demonstrating their consistent superiority in improving traffic efficiency and ensuring the stability of mixed traffic flow.

Methodology

Problem description

This study considers a freeway on-ramp merging scenario, where the road layout consists of a mainline, an on-ramp, and a parallel acceleration lane connecting them, as illustrated in Fig. 1.

The merging area is divided into two functional zones: the Cooperative Control Zone (CCZ) and the Ramp Merging Zone (RMZ). The CCZ is located upstream of the physical merging point, where CAVs receive centralized control instructions via roadside units to perform speed regulation and gap coordination. The RMZ is situated downstream, where vehicles execute lane-changing and merging maneuvers.

Based on the scenario description and problem definition, the cooperative merging problem for the on-ramp vehicle is formulated as a hierarchical cooperative merging framework consisting of the decision-making layer and the optimal control layer. The decision-making layer first determines the cooperative vehicle group (CVG) and the cooperative action to specify the target merging strategy. The selected decision is then mapped into the terminal boundary conditions of the optimal control trajectory planning problem to generate a feasible vehicle trajectory. Such a hierarchical formulation allows the discrete merging strategy and the continuous trajectory generation process to be treated in a structured way.

In this way, the proposed framework simultaneously improves traffic efficiency and preserves traffic flow stability. The mathematical formulation of the cooperative merging problem is given as follows:

$$\min f(X) \tag{1}$$

$$X = \{C_{i,k}, \alpha, u(t)\} \tag{2}$$

$$s.t.$$

$$\alpha \in A$$

$$u_{\min} \le u(t) \le u_{\max}$$

where, $f(X)$ denotes overall objective function of the hierarchical cooperative merging problem; X denotes the set of decision variables. The definitions of key variables and parameters are provided in Table 1.

The resulting trajectory reflects the feasibility of the selected decision and ensures efficient merging behavior. In this way, the overall merging process is realized through a sequential process in which the decision-making layer provides the boundary conditions for the optimal control layer.

Modelling of decision-making layer

The core objective of the decision-making layer is to reshape the traffic flow in the ramp merging area by actively allocating merging gaps. To mathematically formulate this process, we define the state space, the active cooperative action space, and the objective function.

Cooperative vehicle group

In mixed traffic environments, centralized modelling of the entire traffic flow is computationally prohibitive. The optimization process often suffers from the curse of dimensionality. To address this issue, this study proposes a CVG approach, which decouples the global merging problem into multiple localized sub-problems. This method effectively captures local traffic topologies, significantly reduces computational complexity, and lays a solid foundation for subsequent cooperative decision-making.

The modelling process is triggered at time t, when the ramp vehicle r_i enters the CCZ. At this instant, a set of feasible physical gaps exists on the mainline, where each potential merging gap is strictly bounded by a mainline preceding vehicle and a mainline following vehicle. Consequently, the ramp vehicle and the target gap on the mainline collectively form an independent CVG, whose mathematical state is defined in Eq. (3):

$$C_{i,k} = (r_i, g_k) = (r_i, m_{\text{lead},k}, m_{\text{lag},k}) \tag{3}$$

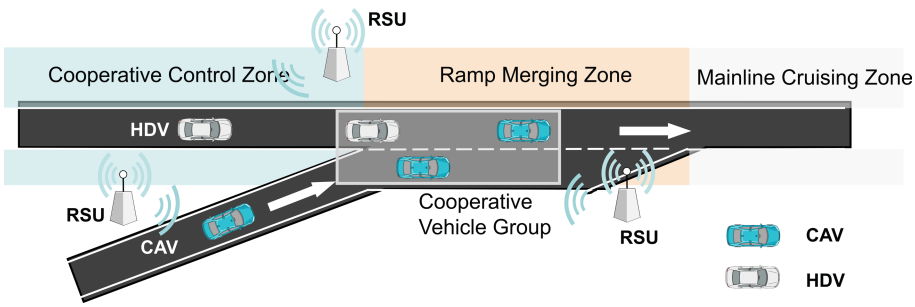

Fig. 1 Freeway on-ramp merging in a mixed traffic environment.

Table 1. Key notations and descriptions of the cooperative merging problem.

Notation	Description
i	Index of the on-ramp vehicle
k	Index of the candidate gap on the mainline
r_i	The i^{th} vehicle originating from the on-ramp
$m_{\text{lead},k}$,$m_{\text{lag},k}$	The leading and lagging vehicles from the k^{th} candidate gap on the mainline
$C_{i,k}$	The cooperative vehicle group corresponding to the on-ramp vehicle r_i for merging into the k^{th} candidate gap
g_k	The k^{th} candidate merging gap on the mainline
$f(X)$	Overall objective function of the hierarchical cooperative merging problem
α	Discrete cooperative action associated with the selected candidate gap on the mainline
A	Set of admissible cooperative actions
t_0,t_m	The initial time and the designated merging time for a vehicle (s)
$t_{\text{rm}}^{\min}$, $t_{\text{rm}}^{\max}$	The earliest and latest achievable time (s) for a vehicle to depart and reach the boundary of the merging area
$x(t)$,$v(t)$,$a(t)$	Longitudinal position (m), speed (m/s), and acceleration (m/s^2)
$v_{\max}$,$v_{\min}$	The maximum and minimum speed (m/s) limits of the road
$a_{\max}$,$a_{\min}$	The maximum acceleration (m/s^2) and maximum deceleration (m/s^2) of the vehicle
$u_{\max}$,$u_{\min}$	The maximum and minimum continuous control input, i.e., jerk (m/s^3)
$u(t)$	Continuous control input, i.e., jerk (m/s^3)
d_{safe}	Minimum safe longitudinal distance (m)
L_{veh}	Standard length of a vehicle (m)
ω_e,ω_s	Weight coefficients for acceleration, and jerk penalties
ω_a,ω_u	Weight coefficients for traffic efficiency and traffic flow stability
J_{decision},J_{control}	Objective functions of the decision-making and optimal control layers
$J_{\text{stability}}$,$J_{\text{efficiency}}$	Sub-objective functions of the traffic flow stability and traffic efficiency
N	Layer of Monte Carlo tree search
Node	Node of Monte Carlo tree search

Cooperative action space

This section constructs an active cooperative action space, denoted as A, based on the CVG type.

Specifically, based on the connectivity status of vehicles within the CVG, the algorithm designs four distinct cooperative action branches: natural merging, follower active deceleration, leader active acceleration, and dual-vehicle cooperation:

$$A = \{\alpha_{\text{NM}},\ \alpha_{\text{FD}},\ \alpha_{\text{LA}},\ \alpha_{\text{DC}}\} \tag{4}$$

where, α_{NM} denotes the natural merging cooperative action; α_{FD} represents the follower active deceleration cooperative action; α_{LA} indicates the leader active acceleration cooperative action; and α_{DC} refers to the dual-vehicle cooperative action.

Each cooperative action $\alpha \in A$ represents a specific interaction strategy, which fundamentally alters the terminal boundary conditions for the subsequent optimal control layer.

(1) Constraints under natural merging:

Only the ramp CAV r_i adjusts its trajectory. The mainline HDVs maintain their predicted constant speeds. The boundary constraints for the ramp vehicle at t_m are:

$$\begin{cases} x_r(t_m) \in \left[x_{\text{lag}}(t_m) + d_{\text{safe}},\ x_{\text{lead}}(t_m) - d_{\text{safe}}\right] \\ v_r(t_m) = v_{\text{des}} \\ a_r(t_m) = 0 \end{cases} \tag{5}$$

(2) Constraints under follower active deceleration:

The lagging CAV actively yields to create space. In addition to the ramp vehicle constraints, the lagging vehicle m_{lag} must reach a specific spatial position to widen the gap by an extra length ΔL_{lag}:

$$\begin{cases} x_{\text{lag}}(t_m) = x_{\text{lead}}(t_{\text{m}}) - L_{\text{gap}} - \Delta L_{\text{lag}} \\ v_{\min} \le v_{\text{lag}}(t_m) \le v_{\max} \\ a_{\text{lag}}(t_{\text{m}}) = 0 \end{cases} \tag{6}$$

(3) Constraints under leader active acceleration:

The leading CAV actively accelerates to create space. The boundary constraint for the leading vehicle m_{lead} is adjusted to provide an extra forward gap ΔL_{lead}:

$$\begin{cases} x_{\text{lead}}(t_m) = x_{\text{lag}}(t_{\text{m}}) + L_{\text{gap}} + \Delta L_{\text{lead}} \\ v_{\min} \le v_{\text{lead}}(t_m) \le v_{\max} \\ a_{\text{lead}}(t_{\text{m}}) = 0 \end{cases} \tag{7}$$

(4) Constraints under dual-vehicle cooperative:

A bidirectional gap-creation maneuver is executed. The terminal boundaries require a synchronized spatial distribution for all three vehicles, satisfying:

$$x_{\text{lead}}(t_m) - x_r(t_m) \ge d_{\text{safe}},\ x_r(t_m) - x_{\text{lag}}(t_m) - L_{\text{veh}} \ge d_{\text{safe}} \tag{8}$$

Objective function of the decision-making layer

An objective function J_{decision} is designed at the decision-making layer to quantitatively assess the chosen candidate gaps on the mainline and the associated cooperative actions. Specifically, the objective is structured to maximize traffic efficiency under severe penalties for traffic oscillations.

$$J_{\text{decision}} = \omega_{\text{e}} J_{\text{efficiency}} + \omega_{\text{s}} J_{\text{stability}} \tag{9}$$

(1) Traffic efficiency $J_{\text{efficiency}}$: this sub-objective is designed to encourage the ramp vehicle to complete merging as early as possible and reduce ramp travel delay, which is quantified by the merging time t_{rm}:

$$J_{\text{efficiency}} = \left| t_{\text{m}}^{\max} - t_{\text{m}} \right| \tag{10}$$

$$s.t.$$

$$t_{\text{rm}}^{\min} \le t_{\text{rm}} \le t_{\text{rm}}^{\max}$$

(2) Traffic flow stability $J_{\text{stability}}$: to maintain the stability of the local mainline traffic flow after merging and suppress traffic oscillations induced by inter-vehicle speed differences, this sub-objective introduces a penalty term for the deviation between the vehicle's speed at the merging instant t_{m} and the desired driving speed v_{des} of the mainline section:

$$J_{\text{stability}} = \sum\nolimits_{n \in C_{i,k}} \left(v(t_{\text{m}}) - v_{\text{des}}\right)^2 \tag{11}$$

$$s.t.$$

$$v_{\min} \le v(t) \le v_{\max}$$

Modelling of the optimal control layer

To describe vehicle longitudinal motion in cooperative merging, each vehicle in the CVG is modelled as a third-order integrator system with jerk as the control input. An optimal control problem is then formulated under kinematic constraints to minimize acceleration and jerk, thereby ensuring smooth trajectories and traffic flow stability.

Vehicle longitudinal dynamics modelling

To accurately describe the dynamic response process of the vehicle effectively, the vehicle is modeled as a third-order integrator system. For any vehicle within the CVG, its state vector $s(t)$ is defined as:

$$s(t) = [x(t),\ v(t),\ a(t)]^T \tag{12}$$

Since jerk (the first derivative of acceleration) directly determines the change rate of acceleration and can describe the dynamic response process of the vehicle more delicately, this paper selects

it as the control input of the system $u(t)$[20]. According to the kinematic differential relationship, the state equation of the system can be expressed in the form of a linear state space, which is specifically expanded as:

$$\dot{s}(t) = [\dot{x}(t),\ \dot{v}(t),\ \dot{a}(t)]^T = [v(t),\ a(t),\ u(t)]^T \tag{13}$$

Subject to the fundamental kinematic constraints:

$$v_{\min} \le v(t) \le v_{\max},\ a_{\min} \le a(t) \le \mathrm{a}_{\max},\ u_{\min} \le u(t) \le u_{\max} \tag{14}$$

Objective function of the optimal control layer

With the system dynamics established, an optimal control objective function J_{control} is formulated to uniquely determine the vehicle trajectory. Guided by the overarching goal of maximizing driving smoothness and mitigating traffic shockwaves, the objective function is designed as a quadratic integral of acceleration and jerk:

$$J_{\text{control}} = \frac{1}{2}\int_{t_0}^{t_m} (\omega_a a(t)^2 + \omega_u u(t)^2)dt \tag{15}$$

$$s.t.$$

$$a_{\min} \le a(t) \le a_{\max}$$

$$u_{\min} \le u(t) \le u_{\max}$$

Solution algorithms: the MCTS-H approach

The hierarchical cooperative merging framework established earlier in this paper effectively decoupled the highly complex mixed-traffic merging problem. However, bridging the gap between discrete decision-making and continuous control inputs necessitates an effective mechanism. To address this, we propose the MCTS-H algorithm, which integrates a kinematically enhanced MCTS with an analytical Hamiltonian-based trajectory solver.

Kinematically enhanced MCTS with kinematic pruning

Lenz et al.[21] applied the conventional MCTS algorithm to optimize merging sequences, demonstrating its effectiveness in decision search. In this study, we redesign the tree expansion mechanism and incorporate a heuristic kinematic pruning strategy into the simulation phase.

Our proposed kinematically enhanced MCTS achieves highly efficient exploration in the state-action space by sequentially executing the following four integrated phases, as shown in Fig. 2:

Phase I: tree policy selection and expansion

Selection step of the algorithm: Starting from the root node, the Upper Confidence Bound (UCB) algorithm is employed to balance the past average reward and future expected reward. The algorithm recursively selects the child node with the highest reward downward until a leaf node is reached. The calculation formula for the UCB algorithm is given by:

$$U = \frac{R_o}{N_o} + C\sqrt{\frac{\ln N_{o,p}}{N_k}} \tag{16}$$

where, U denotes the upper confidence bound value, N_o represents the number of simulations performed at node o, and R_o is the cumulative reward of the node o over N_o simulations. $N_{o,p}$ denotes the number of simulations performed at the parent node of node o; and C is the exploration–exploitation balance factor.

Expansion step of the algorithm: The algorithm initializes a root node to represent the current traffic state. To deal with the high-dimensional cooperative merging scenario, we expand the state-action space using a two-layer tree structure:

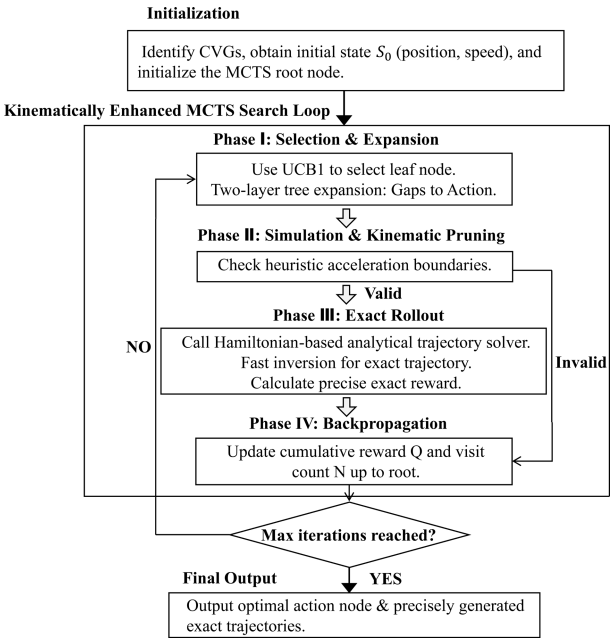

Fig. 2 Flowchart of the kinematically enhanced MCTS algorithm.

Topology selection: In the first layer of the search tree, the proposed kinematically enhanced MCTS algorithm traverses the set of available physical gaps G_i on the mainline at the current time step. For each candidate merging gap in this set, the corresponding CVG $C_{i,k}$ is instantiated as a first-layer node. Let N_{level1} denote the first-layer node set, $\mathrm{Node}_{(C_{i,k})}$ which represents the collection of CVG nodes G_i generated by instantiating each gap g_k in the physical gap set. This set is defined in Eq. (17):

$$N_{\text{level1}} = \{\mathrm{Node}(C_{i,k}) | g_k \in G_i\} \tag{17}$$

where, N_{level1} denotes the set of candidate CVG nodes in the first layer of the kinematically enhanced MCTS search tree, and Node represents the instantiation operator that maps a CVG to an algorithmic state node. At this stage, the search tree completes the preliminary abstraction from the continuous traffic flow environment to the discrete decision target space.

Action allocation: Subsequently, the algorithm iterates through this feasible action subset, instantiating each feasible cooperative action as a candidate action node within the second layer of the search tree. Let N_{level2} denote the set of nodes in the second layer, which comprises all action nodes A_k generated from their respective parent nodes $C_{i,k}$ based on the corresponding action sets. This set is defined as shown in Eq. (18):

$$N_{\text{level2}} = \{\mathrm{Node}(C_{i,k}, \alpha) | g_k \in G_i, \alpha \in A_k\} \tag{18}$$

where, N_{level2} denotes the set of cooperative action nodes in the second layer of the kinematically enhanced MCTS search tree; A_k represents the set of feasible actions pruned based on the CVG's connectivity status; Node is the instantiation operator that combines the CVG and the target action into a tree node; and α refers to a specific cooperative action in the feasible action set A_k. By employing this mechanism, the algorithm realizes on-demand generation of decision branches matched to vehicle capabilities, thereby effectively avoiding invalid searches.

Phase II: simulation and kinematic pruning

This phase acts as a vital computational filter and represents a core innovation of the MCTS-H algorithm. Before triggering the

computationally expensive optimal trajectory solver, the algorithm performs a rapid kinematic feasibility check on the newly expanded action node Node($C_{i,k}$,α).

Assuming the merging instant is t_m, the required spatial boundaries $x(t_m)$ for all involved vehicles in CVG $C_{i,k}$ are rigidly dictated by the assigned action α. To quickly verify physical reachability, the algorithm inversely computes the required heuristic average acceleration $\bar{a}$ based on constant-acceleration kinematics from the initial state [$x(t_0)$,$v(t_0)$]:

$$\bar{a} = \frac{2[x(t_m) - x(t_0) - v(t_0)(t_m - t_0)]}{(t_m - t_0)^2} \tag{19}$$

Pruning rule: The decision branch $C_{i,k}$, α is deemed valid if, and only if there exists at least one feasible merging instant $t_m \in [t_{\min}, t_{\max}]$, such that the heuristic dynamics of all vehicles simultaneously satisfy the fundamental physical boundaries:

$$\begin{cases} a_{\min} \le \bar{a} \le a_{\max} \\ v_{\min} \le v(t_0) + \bar{a}(t_m - t_0) \le v_{\max} \\ \Delta x(t_0) \ge \max(v(t_m) \cdot t_h, d_{\text{safe}}) \end{cases} \tag{20}$$

If any condition in Eq. (21) is violated, it indicates that the action fundamentally exceeds the dynamic limits of the vehicles or poses an imminent collision risk due to HDV uncertainty. In this scenario, the MCTS instantly prunes the branch by assigning a severe penalty reward, thereby entirely avoiding redundant and meaningless searches in invalid state spaces.

Phase III: exact rollout

For the robust decision branches that successfully survive the heuristic pruning filter in Phase II.

Their discrete spatiotemporal boundaries are passed down to the optimal control layer.

Instead of conventional time-consuming numerical simulations or random rollouts to the terminal state, the algorithm directly calls the Hamiltonian-based analytical trajectory solver detailed earlier in this paper.

This controller analytically generates the unique, precise, and jerk-minimized continuous trajectories $s(t)$. Based on these exact trajectories, the precise multi-objective evaluation reward J_{control} is computed to quantify the exact operational reward of the node.

Phase IV: backpropagation

Once the exact evaluation reward J_{control} is obtained from Phase III, this value is backpropagated along the traversed path up to the root node. The cumulative reward Q and the visit count N of all ancestor nodes in the sequence are updated iteratively.

Upon reaching the predefined maximum iteration limit or computational budget, the MCTS-H algorithm terminates and outputs the action node with the highest Q value. This node represents the best cooperative merging decision under the current search budget.

Hamiltonian-based analytical trajectory solver

To address the excessive computational burden caused by the high-frequency solution of continuous optimal trajectories during the exact rollout stage of MCTS-H, this section proposes an analytical Hamiltonian trajectory solver based on Pontryagin's Minimum Principle (PMP), thereby enabling rapid invocation in real-time tree search.

First, by combining the longitudinal state equations with the control objective, the system Hamiltonian is formulated as:

$$H = \frac{1}{2}(\omega_a a(t)^2 + \omega_u u(t)^2) + \lambda_1(t)v(t) + \lambda_2(t)a(t) + \lambda_3(t)u(t) \tag{21}$$

and the optimal control law is obtained from the first-order optimality condition $\frac{\partial H}{\partial u} = 0$ as:

$$\frac{\partial H}{\partial u} = \omega_u u(t) + \lambda_3(t) = 0 \Rightarrow u^*(t) = -\frac{\lambda_3(t)}{\omega_u} \tag{22}$$

Furthermore, according to the co-state equation $\dot{\lambda} = -\frac{\partial H}{\partial x}$, the coupled state–co-state system can be established, through which the original infinite-dimensional variational optimization problem is transformed into a set of first-order ordinary differential equations.

On this basis, by integrating the co-state equations and substituting them into the kinematic relation $\dot{a} = u^*$, the system can be decoupled into a fourth-order linear ordinary differential equation with respect to the position $x(t)$. Its analytical solution can be explicitly expressed in the general form of acceleration, velocity, and position with respect to time, i.e.,

$$a(t),\ v(t),\ x(t) = F(t, k) \tag{23}$$

where, $K = [k_1,k_2,k_3,k_4,k_5,k_6]^T$ is the undetermined coefficient.

Subsequently, by using the initial boundary condition at the triggering time, $s_0 = [x(t_0),\ v(t_0),\ a(t_0)]^T$, and the target boundary condition at the merging time, $s_m = [x(t_m),\ v(t_m),\ 0]^T$, the following linear system can be constructed:

$$P = R(t_0, t_m, W) \cdot K \tag{24}$$

from which the coefficient vector can be obtained directly through matrix inversion as:

$$K = R^{-1}P \tag{25}$$

Therefore, the originally complex continuous vehicle optimal control problem is equivalently transformed into a single 6×6 matrix inversion problem, which significantly reduces the online computational cost.

Once K is determined, the exact trajectory $s^*(t)$ can be generated efficiently, and the multi-objective decision reward J_{decision} can be evaluated accordingly. In this way, an efficient connection is established between macroscopic combinatorial decision-making and microscopic continuous control, thereby supporting real-time cooperative merging optimization.

For a rigorous step-by-step derivation of this Hamiltonian framework in freeway merging scenarios, readers are referred to the established methodologies in Rios-Torres et al.[9] and Zhou et al.[11].

Case study

Simulation experiment

To verify the effectiveness and robustness of the proposed MCTS-H ramp cooperative merging control method, this study conducts simulation verification based on SUMO and Python. SUMO can simulate microscopic vehicle dynamic behaviors and realize real-time control of the underlying vehicles by the upper-layer decision algorithm via the TraCI interface[22].

Simulation parameters

The simulation framework is implemented using SUMO coupled with Python via the TraCI interface. The key simulation settings and scenario configurations are summarized in Table 2. The demand levels and demand splits considered in this study are set according to Han et al.[23]. It must be emphasized that when conducting simulation experiments, the demand levels of the two lanes are summed and split according to the mainline-ramp demand splits.

In the mixed traffic setting, HDVs use the built-in IDM car-following model and LC2013 lane-changing model of SUMO to simulate the random driving behavior of human drivers under perception error and reaction delay. When cooperative control is not activated,

Table 2. Key parameter configuration of simulation platform and scenario settings.

Category	Parameter	Value
Simulation Platform	Simulation duration	180 s
	Simulation step size	0.1 s
Road topology	Mainline length	1,200 m
	Cooperative control zone	600 m
	Merging zone	200 m
	Downstream zone	400 m
	Ramp length	1,000 m
	Acceleration lane	200 m
	Lane width	3.75 m
	Control trigger position	400 m upstream of merge point
Initial conditions	Mainline initial speed	33 m/s
	Ramp initial speed	10 m/s
Traffic flow setting	Arrival distribution	Poisson distribution
	Headway distribution	Negative exponential distribution
	Traffic demand	1,400, 1,800, 2,200 veh/h
	Traffic demand split	50–50, 65–35, 80–20
	CAV penetration rate	20, 40, 60, 80

CAVs adopt the Cooperative Adaptive Cruise Control (CACC) model to maintain a high-precision car-following state. The specific vehicle dynamic parameters and model settings are shown in Table 3.

Key parameter configuration of the MCTS-H algorithm

The performance of the MCTS-H algorithm is highly dependent on the parameters of the search tree and the weight configuration of the objective function. According to the code implementation logic, the algorithm parameters are set to balance computational real-time performance and decision optimality.

To meet the real-time computing requirements of the on-board unit, MCTS limits the maximum number of search iterations and simulation steps. During the solution process of the PMP analytical solution, a corresponding time grid is set to discretize the state space to ensure that the generated trajectory is within the dynamic boundary. The specific algorithm parameter configuration is shown in Table 4.

Results and discussion

This section evaluates the proposed MCTS-H algorithm from both traffic efficiency and traffic flow stability. First, the traffic efficiency is assessed under varying traffic demand levels, demand splits, and CAV penetration rates by comparing MCTS-H with the no-control and Proportional-Integral-Derivative (PID) control baselines. Then, the traffic flow stability is assessed through spatiotemporal trajectory evolution and traffic oscillation characteristics. The PID method is used as a representative reactive baseline, since it regulates merging behavior through local feedback-based speed adjustment and provides a computationally simple benchmark for comparison with the proposed proactive coordination strategy.

Table 3. Key parameter configuration of vehicle kinematics and simulation models.

Parameter	Value
Vehicle length	5.0 m
Standing gap	2.5 m
Maximum acceleration of CAVs	3.5 m/s^2
Maximum acceleration of HDVs	2.5 m/s^2
Minimum deceleration of vehicles	−4.0 m/s^2
Minimum safe time headway	1.5 s
Maximum road speed limit	33.0 m/s
Desired merging speed	20.0 m/s
Initial speed of mainline vehicle	33.0 m/s
Initial speed of ramp vehicle	10.0 m/s
Random noise term	0.5

Table 4. Key parameter configuration of the MCTS-H algorithm.

Parameter	Value
Simulation time step	5.0 s
Maximum search depth	10.0
Exploration constant	1.414
Decision update period	1 s
Weight of efficiency term	0.4
Weight of stability term	0.3
Control weight coefficient of ramp vehicle	1.5
Control weight coefficient of mainline vehicle	2.0
Acceleration weight coefficient	1.0
Jerk weight coefficient	1.0
Weight ratio	0.5
Trajectory planning horizon	5.0

Traffic efficiency evaluation

To comprehensively evaluate the traffic efficiency, this section examines its performance under varying traffic conditions from two perspectives: (1) different demand levels and demand splits, and (2) different CAV penetration rates in mixed traffic. Average speed, total travel time, and average delay are used as the primary performance indicators.

To improve the traceability of the experimental results, the traffic-efficiency evaluation is organized into two groups of scenarios. Tables 5–7 report the results under different demand levels and demand splits at a fixed CAV penetration rate, whereas Figs 3 and 4 present the results under different CAV penetration rates with the demand split fixed at 50–50.

(1) Different demand levels and demand splits:

We first analyzed the effect of demand level and demand split under a 20% CAV penetration rate. As shown in Tables 5–7, MCTS-H consistently outperforms both the no-control and PID baselines across all tested demand intensities and demand splits.

The 50–50 demand split represents the most challenging condition because the balanced mainline and ramp inflows intensify merging interactions and increase conflict pressure. Under this

Table 5. Average travel speed and total travel time under the 50–50 demand split at a 20% CAV penetration rate.

Method	Demand (veh/h)					
	Average travel speed (m/s)			Total travel time (min)		
	1,400	1,800	2,200	1,400	1,800	2,200
No control	20.48	20.15	19.29	156.96	181.07	206.81
PID	23.30	20.64	18.78	141.51	172.91	203.70
MCTS-H	24.89	24.10	22.55	132.94	155.76	181.48

Table 6. Average travel speed and toal travel time under the 65–35 demand split at a 20% CAV penetration rate.

Method	Demand (veh/h)					
	Average travel speed (m/s)			Total travel time (min)		
	1,400	1,800	2,200	1,400	1,800	2,200
No control	20.69	20.58	20.42	132.58	148.81	165.13
PID	23.51	23.45	23.19	119.87	134.22	149.58
MCTS-H	25.33	25.01	24.72	111.73	126.27	140.85

Table 7. Average travel speed and total travel time under the 80–20 demand split at a 20% CAV penetration rate.

Method	Demand (veh/h)					
	Average travel speed (m/s)			Total travel time (min)		
	1,400	1,800	2,200	1,400	1,800	2,200
No control	20.65	20.74	20.64	109.16	117.79	126.98
PID	23.40	23.45	23.49	99.08	107.02	114.80
MCTS-H	25.34	25.36	25.28	91.90	99.38	107.06

condition, MCTS-H maintains the highest average speed and the lowest total travel time across all demand levels. Under a demand increase to 2,200 veh/h, the average speed under MCTS-H remains 22.55 m/s, whereas the PID baseline decreases to 18.78 m/s, which is even lower than that of the uncontrolled case. Meanwhile, the total travel time under MCTS-H is limited to 181.48 min, significantly lower than 206.81 min in the no-control scenario. These results indicate that MCTS-H can reduce merging travel time while improving average travel speed.

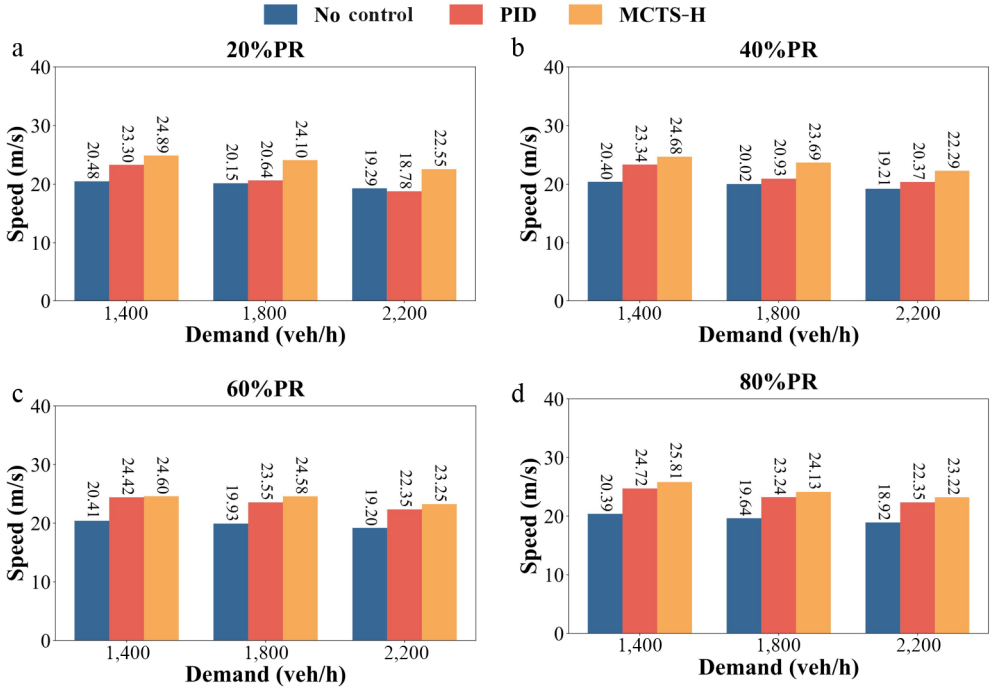

Fig. 3 Comparison of average vehicle speeds across varying traffic demands; (a) results at 20% PR; (b) results at 40% PR; (c) results at 60% PR; (d) results at 80% PR.

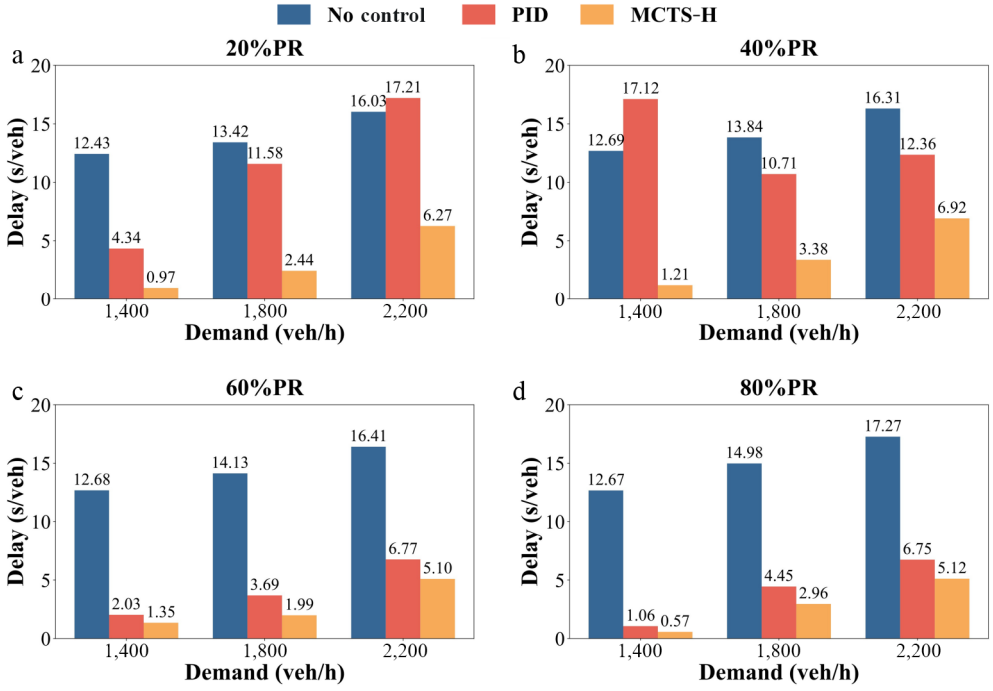

Fig. 4 Average vehicle delay performance under varying traffic demands; (a) results at 20% PR; (b) results at 40% PR; (c) results at 60% PR; (d) results at 80% PR.

When the demand split becomes more asymmetrical, the performance of all methods improves, but MCTS-H still achieves the best overall efficiency. Under the 65–35 demand split, the total travel time under MCTS-H is reduced from 165.13 min in the no-control case to 140.85 min at 2,200 veh/h.

Under the 80–20 demand split, MCTS-H shows the most stable behavior, with the average speed remaining around 25 m/s across all demand levels and the growth of total travel time being substantially smaller than in the other demand-split scenarios. This result suggests that the proposed method not only performs robustly under challenging traffic conditions but also preserves a high performance ceiling under relatively favorable flow configurations.

Having established the effectiveness of MCTS-H across different demand splits, the analysis is further focused on the 50–50 demand split, which represents the most challenging merging condition. Under this setting, the combined effects of traffic demand and CAV penetration rate are examined to evaluate traffic efficiency. Average vehicle speed and average vehicle delay are used as the two core performance metrics. Figure 3 presents the average vehicle speed results, while Fig. 4 shows the corresponding delay results.

(2) Different CAV penetration rates in a mixed traffic environment:

As shown in Fig. 3, the proposed MCTS-H method consistently improves average vehicle speed in the RMZ under mixed-traffic conditions. In particular, under the 60% CAV penetration scenario, MCTS-H achieves the highest average speed at all tested demand levels, reaching 24.60, 24.58, and 23.25 m/s at 1,400, 1,800, and 2,400 veh/h, respectively. Its advantage remains evident under medium and high demand: at 1,800 veh/h, the average speed is improved by 23.33% and 4.37% relative to the no-control and PID methods, respectively, while at 2,400 veh/h, the corresponding improvements are 22.53% and 4.03%. MCTS-H also outperforms the two baselines under other penetration scenarios. For example, under a 40% CAV penetration rate and a traffic demand of 2,400 veh/h, the average vehicle speed is 16.03% and 9.42% higher than those of the no-control and PID methods, respectively. Overall, the average vehicle speed under MCTS-H remains above 22 m/s across all tested mixed-traffic scenarios, indicating stable performance gains and strong adaptability.

Similar advantages can also be observed under the other CAV penetration scenarios. Overall, across different traffic demand levels and penetration rates, MCTS-H consistently maintains higher average vehicle speeds than the no-control and PID baselines, demonstrating robust efficiency gains in mixed-traffic environments.

Figure 4 further confirms the superiority of MCTS-H in terms of delay reduction. Across all tested scenarios, the average vehicle delay under MCTS-H remains below 7 s/veh, and the best performance is achieved at an 80% CAV penetration rate, where the minimum delay is only 0.57 s/veh. In the congested scenario with a 60% CAV penetration rate and a traffic demand of 2,400 veh/h, MCTS-H reduces average vehicle delay by 68.92% and 24.67% compared with the no-control and PID methods, respectively. Another noteworthy observation is that the delay under MCTS-H does not decrease monotonically with increasing CAV penetration in all cases. For example, under a traffic demand of 1,800 veh/h, the delay increases from 2.44 s/veh at a 20% penetration rate to 3.38 s/veh at 40%, and then decreases to 1.99 s/veh at 60%. This non-monotonic trend suggests that, at intermediate penetration levels, interactions between CAVs and HDVs may temporarily amplify behavioral uncertainty. Nevertheless, MCTS-H still achieves the lowest delay among the three methods, indicating strong robustness against congestion and disturbance propagation.

Overall, the above results demonstrate that MCTS-H provides improvements in efficiency under varying demand levels, demand splits, and CAV penetration rates. It not only improves average vehicle speed and reduces total travel time under different flow configurations, but also substantially lowers average vehicle delay in a mixed traffic environment.

Traffic flow stability analysis

To further evaluate the impact of MCTS-H on traffic flow operations, this subsection focuses on traffic flow stability analysis rather than relying solely on macroscopic statistical indicators. Specifically, traffic flow stability is evaluated from the perspective of disturbance suppression and motion smoothness, which is reflected by: (1) whether spatiotemporal trajectories remain continuous and orderly without obvious backward-propagating congestion bands; (2) whether abrupt speed and acceleration fluctuations are effectively reduced during merging; and (3) whether vehicles quickly return to a near-parallel car-following pattern after merging.

Therefore, the stability analysis is organized into three parts: (1) the spatiotemporal trajectory characteristics of MCTS-H under low- and high-demand conditions, to examine its ability to maintain smooth and stable traffic evolution during the merging process; (2) a comparative trajectory analysis of MCTS-H and PID under high traffic demand, to assess their differences in disturbance suppression and traffic flow stabilization; and (3) representative merging cases at the microscopic level, to further illustrate how the proposed control strategy mitigates disturbance propagation and contributes to stable and orderly mixed traffic flow.

(1) Spatiotemporal trajectory characteristics under MCTS-H:

Figure 5 shows the spatiotemporal trajectories in the RMZ under low- and high-demand scenarios for the proposed MCTS-H method. In both cases, the trajectories remain smooth and well-organized throughout the CCZ and the merging area. Under low demand, ramp vehicles merge between adjacent mainline vehicles with only slight trajectory adjustments in the mainline flow. Under high demand, although the trajectories become denser, they remain continuous, with no obvious discontinuities or clustering in the merging zone. In both subfigures, the trajectories of mainline and ramp vehicles quickly return to a nearly parallel pattern after the merger, and no backward-propagating congestion band appears downstream. These observations indicate that MCTS-H can maintain a stable car-following state after merging and confine disturbances to a limited spatiotemporal range.

This improvement in traffic stability can be attributed to the hierarchical control mechanism of MCTS-H. By combining gap-selection decisions and cooperative action with a Hamiltonian-based analytical trajectory solver, the method allows CAVs to execute smooth and proactively coordinated maneuvers in the presence of HDV uncertainty. Instead of relying on reactive local speed adjustments, the controller guides vehicles to follow globally optimized and dynamically feasible trajectories, thereby providing surrounding HDVs with more stable and predictable car-following references. As a result, excessive braking responses triggered by uncertain preceding-vehicle behavior can be reduced, and the amplification of stop-and-go disturbances can be suppressed at an early stage. Overall, the spatiotemporal trajectory analysis under both low- and high-demand conditions confirms that MCTS-H not only improves the performance of ramp merging, but also fundamentally enhances traffic flow stability in the merging zone by mitigating the evolution of microscopic disturbances into traffic oscillations.

(2) Comparative trajectory analysis of MCTS-H and PID under high traffic demand:

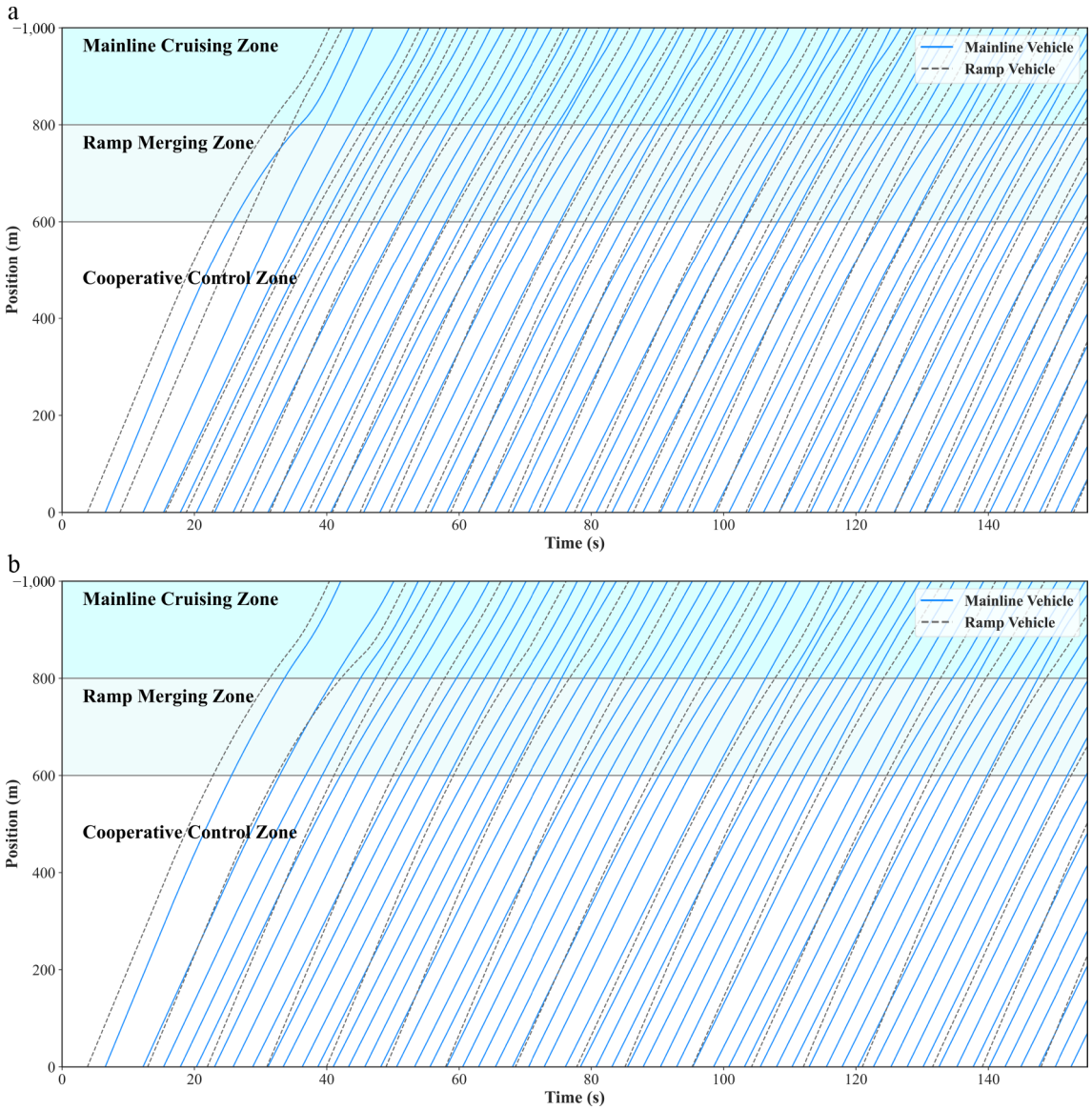

Fig. 5 Spatiotemporal trajectory diagram of vehicles in the on-ramp merging area under the MCTS-H cooperative control method. (a) Low traffic demand scenario. (b) High traffic demand scenario.

To further clarify the difference between MCTS-H and the conventional PID controller under high-density merging conflicts, Fig. 6 presents the spatiotemporal trajectories under PID in the high-demand scenario. Compared with Fig. 5b, a clear difference can be observed. Under MCTS-H, vehicles travel through the CCZ with nearly constant slopes, indicating relatively homogeneous speeds and smooth motion toward the merging point. By contrast, the PID trajectories exhibit noticeable curvature changes, reflecting repeated speed adjustments before merging. This suggests that MCTS-H coordinates merging proactively through gap selection of the decision-making and trajectory smoothing of the optimal control layer, whereas PID relies on reactive local regulation. Under PID, these local adjustments propagate backward over time and form a continuous deceleration influence from approximately 45 to 140 s. Although no severe congestion wave is formed, the resulting speed distribution is less uniform than that under MCTS-H, implying that the traffic stream remains only partially stabilized and is more vulnerable to disturbance amplification. Overall, the comparison between Figs 5b and 6 shows that the superiority of MCTS-H under high traffic demand lies not only in improved performance, but also in its ability to suppress the backward propagation of microscopic disturbances.

By contrast, the PID method exhibits the characteristic behavior of a reactive car-following controller. In the CCZ from 0 to 600 m, the vehicle trajectories under PID display evident curved profiles with gradually changing slopes, indicating alternating acceleration and deceleration. Moreover, these local adjustments propagate backward over time, forming a continuous deceleration influence from approximately 45 to 140 s. This phenomenon arises because the PID controller attempts to preserve time headway and create merging opportunities through local feedback-based speed regulation. Although no severe congestion wave is formed in this case, the resulting speed distribution is clearly less uniform than that under MCTS-H, implying that the traffic stream remains only partially stabilized and is more vulnerable to disturbance amplification.

Overall, the comparison between Figs 5b and 6 demonstrates that the superiority of MCTS-H under high traffic demand lies not only in improved performance, but also in its fundamentally different

control mechanism. Whereas PID responds to conflicts after they emerge, MCTS-H proactively coordinates merging through the hierarchical combination of gap selection and trajectory smoothing. This mechanism promotes more homogeneous traffic evolution, mitigates the backward propagation of disturbances, and prevents microscopic fluctuations from developing into traffic oscillations in the merging zone.

(3) Microscopic cooperative dynamics in representative successful merging cases:

As shown in Fig. 7, the proposed MCTS-H method enables the ramp vehicle to perform active speed regulation that is consistent with both gap selection and smooth merging requirements. Through the embedded pruning strategy based on kinematic constraints, the decision-making layer eliminates dynamically infeasible solutions during the search process and thereby provides the optimal control layer with a physically executable spatiotemporal window. On this basis, the Hamiltonian-based Analytical Trajectory Solver controller ensures the optimal dynamic realization of the selected merging sequence. Specifically, the ramp vehicle accelerates from 10 to 30 m/s during 90–100 s, and then decelerates smoothly between 125 and 145 s, with its acceleration decreasing to about −0.7 m/s^2 and its speed converging to 21 m/s, which is close to that of the adjacent mainline vehicle. This coordinated regulation ensures a stable merging process during 140–150 s. Such a control pattern, namely, accelerating first to match the target gap and then decelerating smoothly to achieve speed synchronization. In this way, infeasible merging attempts caused by excessive speed differences can be effectively avoided.

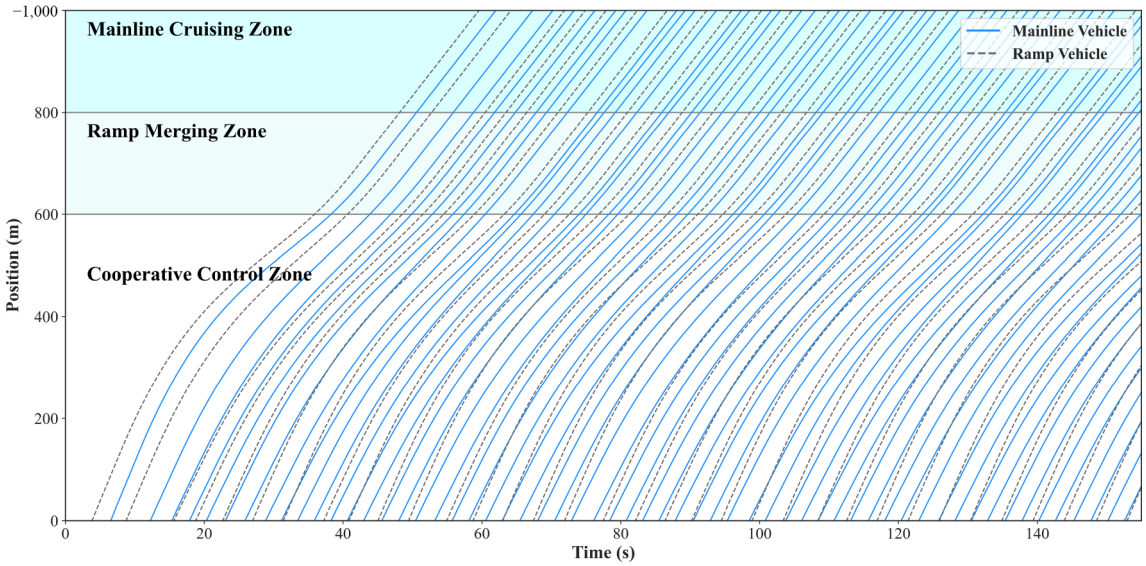

Fig. 6 Spatiotemporal trajectory diagram of vehicles in the on-ramp merging area under the PID method.

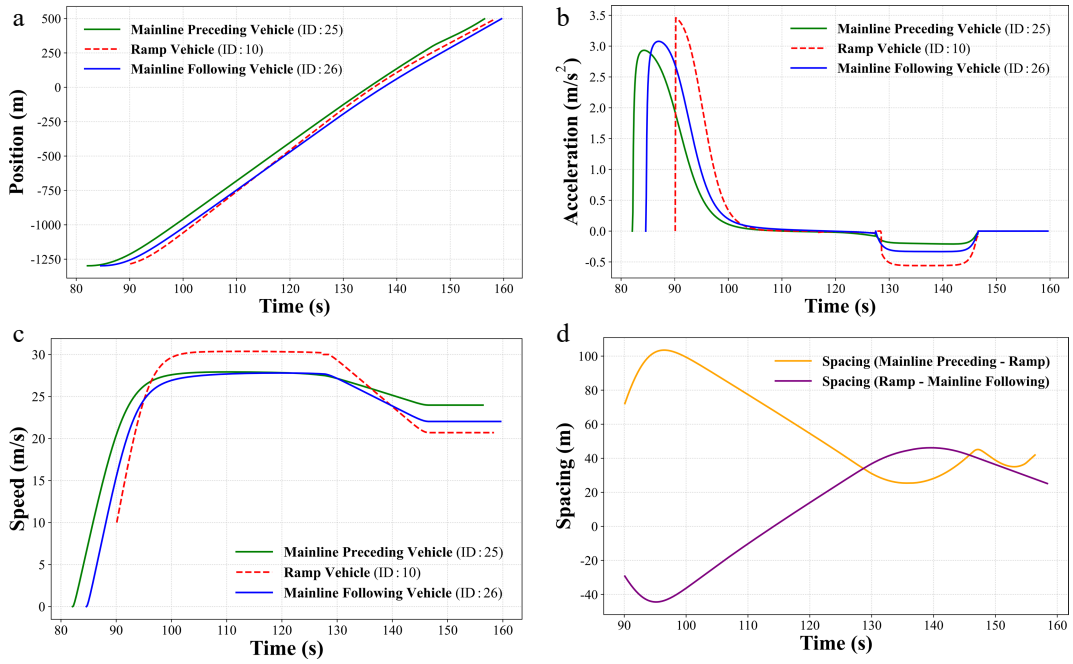

Fig. 7 Cooperative trajectories and dynamic characteristics analysis of three vehicle groups under the MCTS-H cooperative control method; (a) longitudinal position trajectories; (b) acceleration profiles; (c) speed profiles; (d) evolution of inter-vehicle spacing.

At the same time, the mainline vehicles also execute cooperative speed regulations to actively create a feasible gap for the ramp vehicle. As shown in Fig. 7b, c, the following mainline vehicle begins an active gap-creation maneuver at approximately 125 s, with its acceleration profile exhibiting a smooth depression near 130 s and its speed decreasing from 27 to 22 m/s. Meanwhile, the preceding mainline vehicle performs a smaller-amplitude deceleration over the same period, with its speed decreasing from 27 to 24 m/s. This behavior provides direct evidence that MCTS-H does not merely optimize the ramp vehicle trajectory alone, but instead coordinates both ramp and mainline vehicles based on the upper-layer decision outcome. By issuing cooperative control actions to the mainline vehicles, the algorithm enables them to yield proactively and create a more adaptable merging opportunity, thereby realizing truly bidirectional cooperation between the ramp stream and the mainline flow.

In addition to the three-vehicle case, a two-vehicle cooperative control scenario may arise when no suitable leading or following mainline vehicle can be matched. To verify the robustness of the proposed method under such special conditions, Fig. 8 presents a representative two-vehicle cooperative merging case under a traffic demand of 2,200 veh/h with a 50–50 demand split. The results show that MCTS-H can still achieve effective decision-making in a scenario involving only two interacting vehicles. During 120–160 s, the ramp vehicle accelerates to 30 m/s and maintains this speed for approximately 30 s, which rapidly reduces the relative distance to the mainline vehicle and shortens the merging time. During 160–180 s, the algorithm continues to pursue efficiency while strictly satisfying the car-following safety constraint. After approximately 155 s, the ramp vehicle and the mainline vehicle perform synchronized cooperative decelerations, with their speeds gradually converging to 22 m/s, while the inter-vehicle distance is maintained within a safe range of about 40 m. This case further confirms that MCTS-H can transform the decision into smooth microscopic control actions and ensure traffic flow stability.

This case further demonstrates that MCTS-H can accurately transform the optimal decision into smooth microscopic control through the coordinated regulation of vehicle speed and acceleration. By synchronizing the maneuvers of the ramp vehicle and the mainline vehicle, the algorithm effectively reduces abrupt speed changes, enhances merging coordination, and ensures traffic flow stability can be achieved at the microscopic interaction level.

Conclusions

This study proposes a hierarchical control framework for cooperative on-ramp merging, consisting of a decision-making layer and an optimal control layer. To efficiently solve the formulated problem, the MCTS-H algorithm is developed. The findings of this study demonstrate that the proposed hierarchical control framework and MCTS-H algorithm provide an effective solution for cooperative on-ramp merging in mixed traffic environments. From the perspective of traffic efficiency, MCTS-H consistently enhances traffic efficiency across a wide range of traffic demands, demand splits, and CAV penetration rates. From the perspective of traffic flow stability, MCTS-H effectively suppresses traffic oscillations induced by HDV maneuvers, leading to smoother spatiotemporal evolution and reduced disturbance propagation. As a result, a more stable traffic flow is achieved. Overall, the proposed method successfully enhances both traffic efficiency and flow stability, demonstrating strong robustness and applicability for cooperative merging control.

Despite the promising results, the current framework is more suitable for single-lane, single-ramp freeway merging scenarios, where the dominant challenge is local longitudinal conflict resolution under mixed traffic conditions. Its direct application to more complex traffic environments may still be constrained by simplified HDV behavior modeling and the exclusion of lateral interactions. Therefore, further extension and validation are needed before deployment in multi-lane or multi-ramp scenarios with stronger interaction complexity.

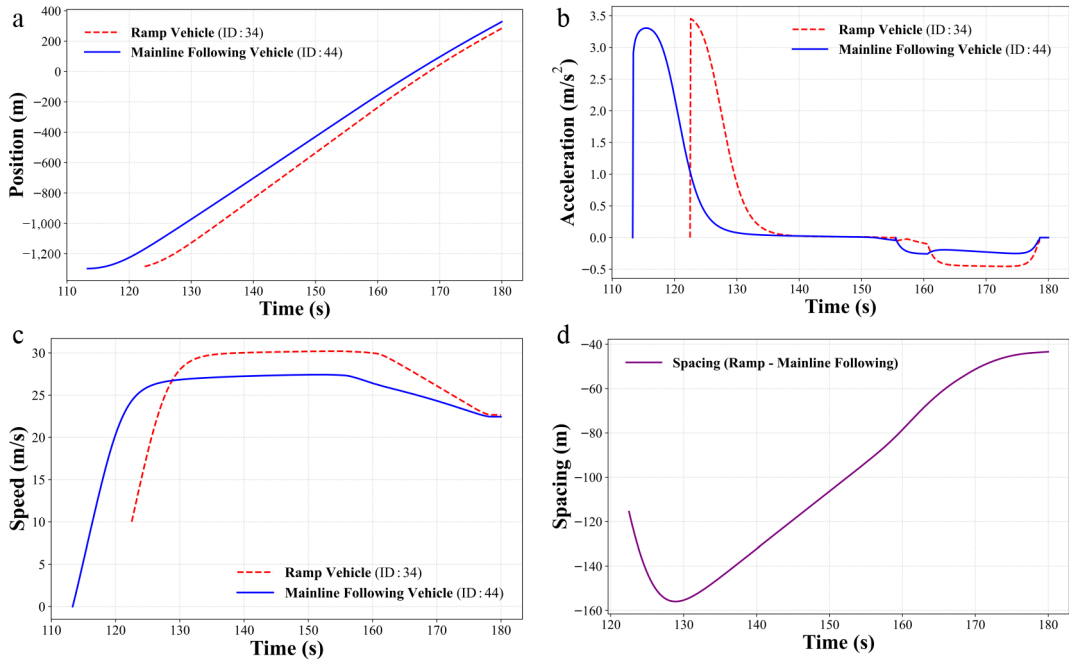

Fig. 8 Cooperative trajectories and dynamic characteristics analysis of two vehicle groups under the MCTS-H cooperative control method; (a) longitudinal position trajectories; (b) acceleration profiles; (c) speed profiles; (d) evolution of inter-vehicle spacing.

Future work will first focus on extending the framework to multi-lane and multi-ramp scenarios, and then incorporate more realistic human driving behavior, communication delays, sensor uncertainty, and lane-changing dynamics.

Author contributions

The authors confirm contributions to the paper as follows: study conception and design: Wang T, Deng H; data collection: Ning W, Fang Y, Li J; analysis and interpretation of results: Wang T, Deng H, Luo Y; draft manuscript preparation: Wang T, Deng H. All authors reviewed the results and approved the final version of the manuscript.

Data availability

The datasets generated and/or analyzed during this study are available from the corresponding author upon reasonable request.

Acknowledgments

This work was supported by the Guangxi Key Research and Development Program (Grant Nos AB25069333, AD25069109) and the National Natural Science Foundation of China (Grant No. 52262047).

Conflict of interest

The authors declare that they have no conflict of interest.

Dates

Received 24 March 2026; Revised 13 April 2026; Accepted 27 April 2026; Published online 29 June 2026

References

[1] Kondyli A, Elefteriadou L. 2011. Modeling driver behavior at freeway–ramp merges. *Transportation Research Record: Journal of the Transportation Research Board* 2249:29–37

[2] Carlson RC, Manolis D, Papamichail I, Papageorgiou M. 2012. Integrated ramp metering and mainstream traffic flow control on freeways using variable speed limits. *Procedia - Social and Behavioral Sciences* 48:1578–1588

[3] Liu H, Zhuang W, Yin G, Li R, Liu C, et al. 2021. Decentralized on-ramp merging control of connected and automated vehicles in the mixed traffic using control barrier functions. *Proc. 2021 IEEE International Intelligent Transportation Systems Conference (ITSC), Indianapolis, IN, USA, 2021*. US: IEEE. pp. 1125–1131 doi: 10.1109/ITSC48978.2021.9564646

[4] Chen N, van Arem B, Alkim T, Wang M. 2021. A hierarchical model-based optimization control approach for cooperative merging by connected automated vehicles. *IEEE Transactions on Intelligent Transportation Systems* 22:7712–7725

[5] Ding J, Li L, Peng H, Zhang Y. 2020. A rule-based cooperative merging strategy for connected and automated vehicles. *IEEE Transactions on Intelligent Transportation Systems* 21:3436–3446

[6] Hou K, Zheng F, Liu X, Guo G. 2023. Cooperative on-ramp merging control model for mixed traffic on multi-lane freeways. *IEEE Transactions on Intelligent Transportation Systems* 24:10774–10790

[7] Peng R, Yang M, Tao R, Zhang M, Zhang R. 2025. Hierarchical control strategy for cooperative on-ramp merging of connected and automated vehicles on multilane highways. *IEEE Internet of Things Journal* 12(16):34513–34527

[8] Li S, Zhou Y, Ye X, Jiang J, Wang M. 2025. Sequencing-enabled hierarchical cooperative CAV on-ramp merging control with enhanced stability and feasibility. *IEEE Transactions on Intelligent Vehicles* 10(1):65–80

[9] Rios-Torres J, Malikopoulos A, Pisu P. 2015. Online optimal control of connected vehicles for efficient traffic flow at merging roads. *Proc. 2015 IEEE 18th International Conference on Intelligent Transportation Systems, Gran Canaria, Spain, 2015*. US: IEEE. pp. 2432–2437 doi: 10.1109/ITSC.2015.392

[10] Hu X, Sun J. 2019. Trajectory optimization of connected and autonomous vehicles at a multilane freeway merging area. *Transportation Research Part C: Emerging Technologies* 101:111–125

[11] Zhou Y, Cholette ME, Bhaskar A, Chung E. 2019. Optimal vehicle trajectory planning with control constraints and recursive implementation for automated on-ramp merging. *IEEE Transactions on Intelligent Transportation Systems* 20:3409–3420

[12] Zhou Y, Chung E, Bhaskar A, Cholette ME. 2019. A state-constrained optimal control based trajectory planning strategy for cooperative freeway mainline facilitating and on-ramp merging maneuvers under congested traffic. *Transportation Research Part C: Emerging Technologies* 109:321–342

[13] Zhao Z, Wu G, Wang Z, Barth MJ. 2020. Optimal control-based eco-ramp merging system for connected and automated vehicles. *Proc. 2020 IEEE Intelligent Vehicles Symposium (IV), Las Vegas, NV, USA, 2020*. US: IEEE. pp. 540–546 doi: 10.1109/IV47402.2020.9304709

[14] Chen J, Zhou Y, Chung E. 2024. An integrated approach to optimal merging sequence generation and trajectory planning of connected automated vehicles for freeway on-ramp merging sections. *IEEE Transactions on Intelligent Transportation Systems* 25:1897–1912

[15] Ntousakis IA, Nikolos IK, Papageorgiou M. 2016. Optimal vehicle trajectory planning in the context of cooperative merging on highways. *Transportation Research Part C: Emerging Technologies* 71:464–488

[16] Xue Y, Ding C, Yu B, Wang W. 2022. A platoon-based hierarchical merging control for on-ramp vehicles under connected environment. *IEEE Transactions on Intelligent Transportation Systems* 23:21821–21832

[17] Yang W, Dong C, Chen X, Chen Y, Wang H. 2023. A cooperative control method for safer on-ramp merging process in heterogeneous traffic flow. *Accident Analysis & Prevention* 193:107324

[18] Cheng G, Chen Y, Wang W, Xu L. 2025. 异质交通流下高速公路 CAV 合流次序优化与轨迹规划方法 [Merging order optimization and trajectory planning methods for highway CAVs in heterogeneous traffic flow]. *北京交通大学学报 [Journal of Beijing Jiaotong University]* 49(1):100–109 (in Chinese)

[19] Huang Z, Fang H, Lin Y, Hu X. 2025. A review of vehicle lane change decisions in human–machine mixed driving environments. *Digital Transportation and Safety* 4:298–311

[20] Liu H, Wang T, Li W, Ye X, Yuan Q. 2024. Lane-change intention recognition considering oncoming traffic: novel insights revealed by advances in deep learning. *Accident Analysis & Prevention* 198:107476

[21] Lenz D, Kessler T, Knoll A. 2016. Tactical cooperative planning for autonomous highway driving using Monte-Carlo Tree Search. *Proc. 2016 IEEE Intelligent Vehicles Symposium (IV), Gothenburg, Sweden, 2016*. US: IEEE. pp. 447–453 doi: 10.1109/IVS.2016.7535424

[22] Gong Y, Zhong S, Zhao S, Xiao F, Wang W, et al. 2025. Optimizing green splits in high-dimensional traffic signal control with trust region Bayesian optimization. *Computer-Aided Civil and Infrastructure Engineering* 40:741–763

[23] Han L, Zhang L, Guo W. 2023. Multilane freeway merging control via trajectory optimization in a mixed traffic environment. *IET Intelligent Transport Systems* 17:1891–1907